Universal scaling laws of quantum spatial search in complex networks

Rei Sato, 1, 2, * Tetsuro Nikuni, 1 Kayoko Nohara, 2 Giorgio Salani, 2 and Shohei Watabe 1, 3, †

1 Department of Physics, Tokyo University of Science, Shinjuku, Tokyo, 162-8601, Japan

2 Department of Transdisciplinary Science and Engineering,

School of Environment and Society, Tokyo Institute of Technology,

2-12-1 O-okayama, Meguro-ku, Tokyo 152-8550, Japan

3 Faculty of Engineering, Computer Science and Engineering,

Shibaura Institute of Technology, Toyosu, Tokyo, 135-8548, Japan

Since quantum spatial searches on complex networks have a strong network dependence, the question arises whether the universal perspective exists in this quantum algorithm for complex networks. Here, we uncover the universal scaling laws of the quantum spatial search on complex networks such as small-world and scale-free networks. The average path length, a key quantity in the complex network science, is useful to expose this universal feature, where the collapse plot can be generated for the optimal time, the maximal finding probability and the optimal hopping parameter. Based on the path integral method, we also clarify that the probability amplitude in the continuous-time quantum walk can be determined by the path length distribution. Our results demonstrate a new link between the quantum physics and the complex networks.

The network science, which is a cornucopia of non-trivial properties covering a wide range of fields, such as classical physics, society, biology and artificial intelligence [1–8], is now intimately involved in the quantum world [9]. Indeed, the complex network science is helpful to understand the real society, for example, the community detection [10, 11], the cascade control [12], and contagion phenomena [13]. However, the scope is now mutually expanding into quantum random networks [14], quantum sensing networks [15, 16], quantum communication [17], entanglement percolation [18, 19], and quantum internet [20–23].

This network science is a fountain of nontrivial concepts behind the complexity. In particular, the classical network science not only provides the concepts of the structure of networks, such as random [24, 25], smallworld [2, 26], scale-free [1, 27] and self-similar [3, 28, 29] networks, but also reveals the dynamical properties [30–34]. Interestingly, notions of the complex network science have also been applied to appreciate quantum systems, such as quantum phase transitions [35], time crystals [36], and localization/delocalization [37, 38]. Tools to analyze the complex networks are also multi-disciplined ranging from the graph theory [7, 8] to the percolation [26], Bose–Einstein condensation [39], random matrix [40], renormalization [41], the quantum annealing [42], quantum walks [43–54], for example.

Indeed, the quantum walk, which has been recently demonstrated in experiments [55–58], is a method widely used in the complex network science, such as the community detection [44, 45], link prediction [47, 48], centrality testing [50, 51], an element ranking [49] and neural networks [46]. In particular, the quantum spatial search using the quantum walk has been extensively investigated for various network structures, e.g., regular lattices [52, 59–61], random graphs [62–64], fractal lattices [65–70], and complex networks [71, 72].

One of the central issues in the quantum spatial search is to reveal the relation between the quantum algorithm and the network structure, such as the scaling relation between the optimal number of oracle calls Q and the number of nodes N, where the scaling $Q = \mathcal{O}(N^{1/2})$ holds in the complete graph [59] and conditionally in the Erdös-Rényi random graph [62], whereas the scaling depends on the spectral dimension in the fractal lattices [67, 68, 70] and on the closeness centrality in the scale-free network [72]. Because of the complexity, the scaling of the optimal number of oracle calls Q depends on the structure of the complex network. The natural question, therefore, arises whether a universal perspective exists in this quantum algorithm for the complex network. Its existence provides a crucial understanding of quantum systems and quantum algorithms in complex networks.

Here we uncover universal properties behind the quantum spatial search in complex networks. The scaling with respect to the number of nodes shows the network dependence, which indicates that such a conventional analvsis is useless to obtain the universal perspective. However, the average path length, which is a key quantity in the complex network science, is found to be crucial in generating collapse plots for various kinds of complex networks, such as small-world networks, the scale-free networks, as well as random, ring and fractal networks. Furthermore, we unveiled a class of networks, including not only the complex network model, such as the Watts-Strogatz (WS) model, but also real-world networks, e.g., co-authorship as well as human disease and mouse brain networks, where the finding probability and the optimal hopping parameter are correlated and those data can be collapsed. Our results provide a new insight into the connection between quantum physics and complex-network science, and will facilitate further integration of these fields.

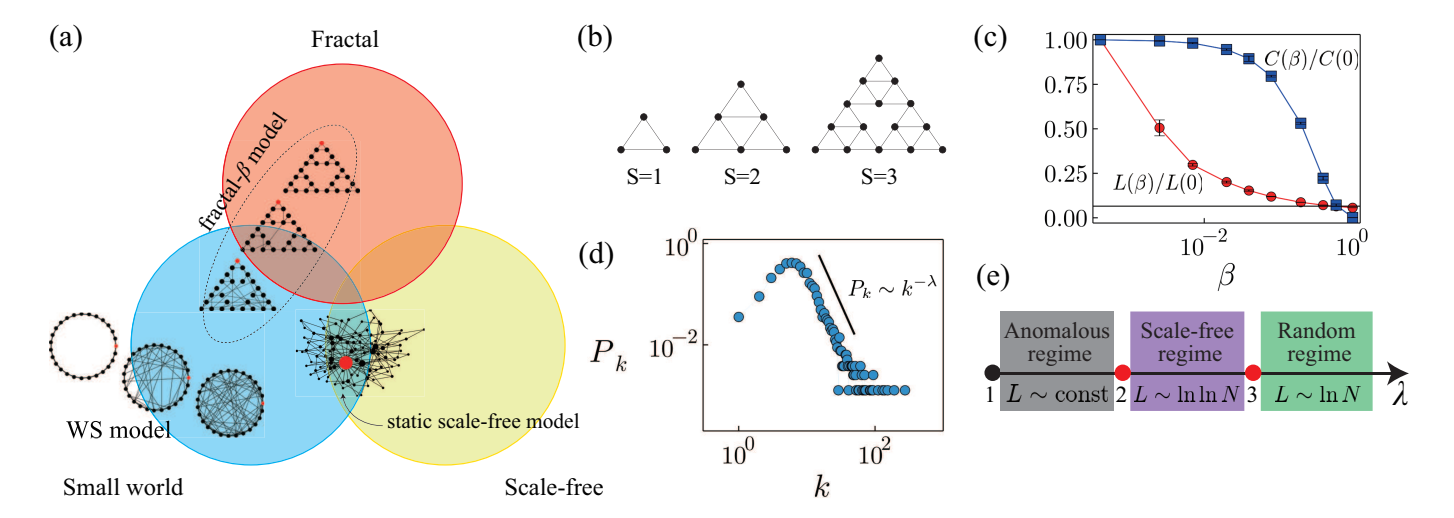


Figure 1. (Color online) (a) A diagram of three characteristic structures of complex networks: small-world, scale-free and fractal networks, which can be covered by the Watts–Strogatz (WS) model, static scale-free model and fractal- β model. (b) Fractal network (fractal- β model with $\beta=0$) at stages S = 1-3. (c) The average path length $L(\beta)$ and average clustering coefficient $C(\beta)$ for the fractal- β model at S=8, where β is a probability of rewiring edges. The solid horizontal line indicates the path length of small-world network $L(\beta) \sim \ln N$. (d) The distribution of the degree in the static scale-free networks for $N=3000, \ \lambda=3$ and the mean degree $\langle k \rangle=6$. The solid line shows the scaling of $P_k \sim k^{-\lambda}$. (e) Three characteristic regimes of the scale-free networks, such as the anomalous regime for $\lambda<2$, scale-free regime with an ultra-small world property for $2<\lambda<3$, and random regime with a small-world property for $\lambda>3$ [73].

To tackle to unveil the universality of the quantum spatial search in complex networks, it is inevitable to prepare various kinds of complex networks, such as regular, random, fractal, scale-free, and small-world networks. We therefore utilize three models: the WS model [2], the fractal- β model with the Sierpinski gasket [74], and the static scale-free network model [75] (Fig. 1 (a)).

The generation of the small-world network is achieved by using the WS model [2] and fractal β model [74]. In the WS model, starting with a ring network, each link is rewired to a randomly chosen node for a probability β [2, 7]. This model can describe the crossover from the regular ring graph at $\beta = 0$ to the random graph at $\beta = 1$ through the small-world network. The fractal- β model also shows the crossover from a fractal lattice at $\beta = 0$, such as the Sierpinski gasket, to the random graph at $\beta = 1$ through the small-world network, where each link is randomly rewired to a node for a probability β [74]. For regular fractal lattices at $\beta = 0$, the scaling of the quantum spatial search was investigated by changing the stage S [67, 68] (Fig. 1 (b)).

The small-world property is characterized by high clustering and a low average path length, where the cluster coefficient has a scaling $C(\beta) = O(N^0)$ [7] and the path length $L(\beta) = O(\ln N)$ for networks with N nodes (Fig. 1 (c)). Here, the average path length is defined as $L = \sum_{i < j}^{N} L_{i,j}/NC_2$, where $L_{i,j}$ is the shortest path between nodes i and j [7]. The average clustering coefficient C is defined as $C = \sum_{i=1}^{N} C_i/N$, where C_i is a local clustering coefficient [7].

The scale-free networks can be generated by using the Barabási-Albert model [1] and the static network models [75–78]. The Barabási-Albert model, or the growing network model, utilizes a growth process to produce the scale-free network, where new nodes and edges are sequentially added to the network following a dynamical rules [1]. Therefore, to simply control the number of nodes N to generate the scale-free network, we employ the static scale-free network models [75], where N is constant and links are wired following stochastic rules.

The scale-free network is characterized by the powerlaw degree distribution $P_k \sim k^{-\lambda}$ (Fig.1 (d)). For $\lambda < 2$, the network is in an anomalous regime with a hub-andspoke structure, where all the nodes are connected to a hub (Fig.1 (e)). For $2 < \lambda < 3$, the network is in the scale-free regime with an ultra-small-world property, whereas for $\lambda > 3$, the network is in a random regime with a small-world property. At $\lambda = 2, 3$, the critical points emerge.

The continuous-time quantum walk on a graph G(V,E) takes place in an N-dimensional Hilbert space enclosed by states $|i\rangle$ with a node label i=1,2,...,N [59]. Here, the graph G is a connected, undirected network with N-vertices and no self-loop. The quantum spatial search is achieved by utilizing the Schrödinger dynamics with the time-independent Hamiltonian $\hat{H}=\hat{H}_L+\hat{H}_w$. Here, $\hat{H}_L\equiv\gamma\hat{L}$ is the Hamiltonian that describes the diffusion or hopping, where γ is a hopping parameter with a positive real number and $\hat{L}\equiv\hat{D}-\hat{A}$ is a Laplacian operator. The operator \hat{D} is a degree operator $\hat{D}=\sum_i d_i|i\rangle\langle i|$

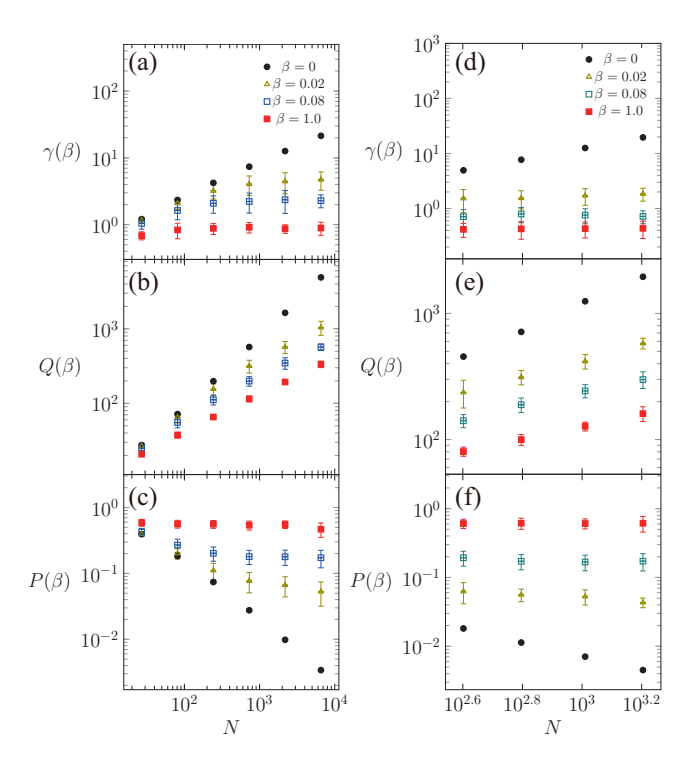


Figure 2. (Color online) Conventional plots of the optimal hopping parameter γ , the optimal time Q and the optimal finding probability P as a function of the number of nodes N in the fractal- β model (a)-(c), and in the WS model (d)-(f), respectively

with the degree d_i for a node i, which is the number of connections to other nodes, and \hat{A} is an adjacency operator $\hat{A} = \sum_{i,j} A_{ij} |i\rangle\langle j|$ with an adjacency matrix A_{ij} . The oracle Hamiltonian \hat{H}_w is given by $\hat{H}_w = -\gamma_w |w\rangle\langle w|$, where w is a target node, and γ_w is a positive real number, which is normalized as unity, i.e., $\gamma_w = 1$.

An initial state for the quantum spatial search is a uniform superposition state, given by $|s\rangle = \sum_{i=1}^N |i\rangle/\sqrt{N}$. The finding probability P(t) at a time t on a target node w is $P(t) = |\langle w| e^{-i\hat{H}t} |s\rangle|^2$. In the quantum spatial search, the hopping parameter γ is optimized so that the peak value of the finding probability is maximized [59]. This condition well corresponds to the condition where the overlap between $|s\rangle$ and the ground state $|E_0\rangle$ of \hat{H} is equal to that for the first-excited state $|E_1\rangle$ [59], i.e., $|\langle s|E_0\rangle|^2 = |\langle s|E_1\rangle|^2 \sim 0.5$. (Hereafter, γ is denoted as the optimal value for simplicity.) Using this optimal γ , we determine the optimal finding probability P as well as the optimal time t=Q, which gives the peak value of the finding probability and its peak-to-peak period, respectively.

Universal perspectives cannot be obtained if the conventional analysis of the quantum search algorithm is employed, where the scaling relations are supposed as $\gamma = \mathcal{O}(N^{a\gamma}), \ Q = \mathcal{O}(N^{aQ}), \ \text{and} \ P = \mathcal{O}(N^{aP})$ (Fig. 2). The network shows the crossover from the regular to ran-

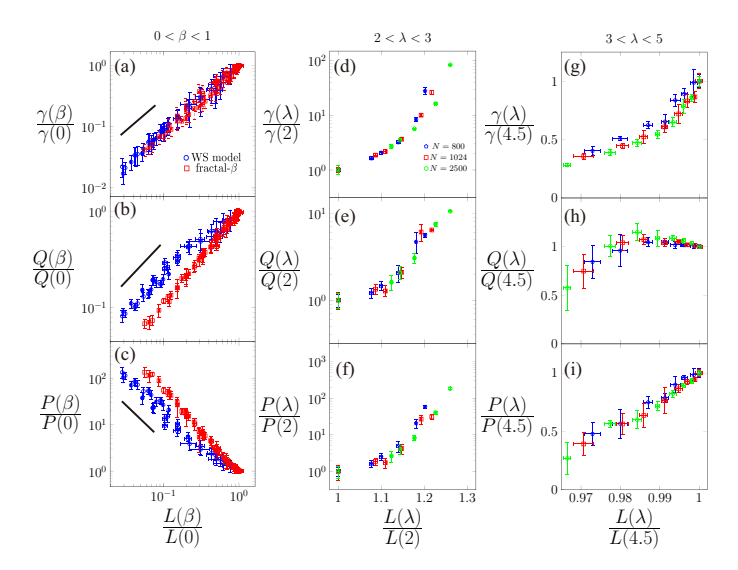


Figure 3. (Color online) Path-length dependence of γ , Q and P in the WS model and fractal- β model (a)-(c), where all the quantities are normalized with each quantity of the regular network ($\beta=0$) with the same number of nodes N. Figures (d)-(f) are for the static scale-free model in the scale-free regime (2 < λ < 3), and (g)-(i) are in the random regime (3 > λ), where a target node is a hub (a node with the maximum degree) and quantities are normalized with those at $\lambda_0=2$ and 4.5, respectively.

dom graphs through the small-world network in the WS model as well as the fractal- β model. The exponents $\alpha_{\gamma,Q,P}$ therefore depend on the parameter β as well as the network models, which is also the case for the static scale-free model with the parameter λ giving the anomalous, scale-free and random regimes. Moreover, in the fractal- β model, strictly speaking, γ , Q and P are not exactly a power function of N except for $\beta=0$ (Figs. 2 (a)-(c)).

Here we seek a universal perspective applicable to complex networks. The quantum spatial search reflects global structures of the complex network, because the initial state is the equal superposition state $|s\rangle$, and the wave function spreads across the complex network throughout the quantum search process. It would be interesting to employ a length scale that characterizes the entire system, inspired by the context of the universality in the continuous phase transition in the statistical physics [79]. A possible characteristic length is an average path length L, rather than a path length between two specific nodes.

Figure 3 shows the average path length dependence of γ , Q and P, where the data for various numbers of sites and various values of parameters β and λ are integrated. In Fig. 3, the data for the WS and fractal- β models were normalized with data for the regular network ($\beta=0$) with the same number of nodes N. For the static scale-free model, the data were normalized with data for a specific value of λ . By these normalizations, we can

surprisingly and successfully generate collapse plots. We have also tried to make similar plots as a function of the average clustering coefficient, for which we could not find any collapse plots in contrast to the case for the average path length. As a result, the average path length, not the average clustering coefficient, is a key to exposing the universality of the quantum spatial search in the complex network.

The collapse plots for the small-world models have the model dependence (Figs. 3 (a)-(c)). The model-specific behavior emerges around $\beta=0$, where the regular lattice structure, such as the ring network and the fractal network, is dominant. In the small-world network regime and random network regime, however, the exponents are common between the WS model and the fractal- β model. Indeed, we have the following scaling law for the WS model and fractal- β model, given by

$$\frac{\gamma(\beta)}{\gamma(0)} = \left(\frac{L(\beta)}{L(0)}\right)^{\alpha_{\gamma}},\tag{1}$$

$$\frac{Q(\beta)}{Q(0)} = \left(\frac{L(\beta)}{L(0)}\right)^{\alpha_Q},\tag{2}$$

$$\frac{P(\beta)}{P(0)} = \left(\frac{L(\beta)}{L(0)}\right)^{\alpha_P},\tag{3}$$

where $\alpha_{\gamma} = 1.08(6)$, $\alpha_{Q} = 0.90(5)$, and $\alpha_{P} = -1.76(8)$.

The average-path-length plot is still efficient for generating the collapse plots in the scale-free network, whereas the L-dependence is completely different in the scalefree regime (Figs. 3 (d)-(f) for $2 < \lambda < 3$) and the random regime (Figs. 3 (g)-(i) for $\lambda > 3$). The average path length dependence clearly emerges in γ , Q and P if the target is a hub, whereas its dependence is weak or absent for a target with a small degree. Although the averagepath-length dependence is completely different between the scale-free network and the small-world network, we can surprisingly generate the collapse plot by utilizing the average path length in both networks. Since the results with various sizes of networks are depicted in a single curve, our results on the universality will be useful to predict the behavior of the quantum spatial search in a huge complex network that cannot be simulated in classical computers by employing a small-size network that is tractable in classical computers.

The rigorous mathematical proof on the path-length scaling law is, unfortunately, still open. However, we can expose the physics behind this by showing an explicit relation between the quantum spatial search and the path length in the complex network. Consider the probability amplitude for the quantum spatial search, given by $\pi \equiv \langle w|e^{-i\hat{H}t}|s\rangle$, where we divide the Hamiltonian $H = \hat{H}_L + \hat{H}_w$ as $H \equiv \hat{H}_A + \hat{H}_d$ with $\hat{H}_A \equiv -\gamma \hat{A}$ and $\hat{H}_d \equiv -\sum_i \Gamma_i |i\rangle \langle i|$ for $\Gamma_i \equiv \gamma_w \delta_{i,w} - \gamma d_i$. By following the path-integral formalism with the Suzuki-Trotterization $\pi(t) = \lim_{M \to \infty} \langle w|(e^{-i\hat{H}_A t/M} e^{-i\hat{H}_d t/M})^M|s\rangle$,

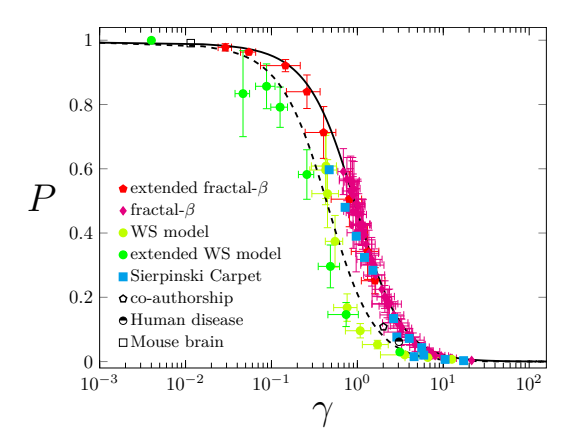


Figure 4. The correlation between the optimal hopping parameter γ and the finding probability P for the (extended) fractal- β model, (extended) WS model, Sierpinski carpet, and networks of the co-authorship [80], human disease [81] and mouse brain [82]. The target node is chosen as a node with a minimum degree. The solid and dashed lines are the fitting function (7) for D=1 and D=2.11(1), respectively.

the probability amplitude π can be decomposed into a kernel $\mathcal{K}_M(i,j;t) \equiv \langle i|e^{-i\hat{H}_At/M}e^{-i\hat{H}_{\rm d}t/M}|j\rangle$, which is reduced into

$$\mathcal{K}_{M}(i,j;t) = e^{i\Gamma_{j}t/M} \sum_{n=0}^{\infty} \frac{1}{n!} \left(\frac{i\gamma t}{M}\right)^{n} P_{n}(i,j). \tag{4}$$

Here, $P_n(i,j)$ is the path length distribution of the path length n from the node j to i, which is given by [8]

$$P_n(i,j) = \langle i|\hat{A}^n|j\rangle. \tag{5}$$

As a result, the probability amplitude can be related to the path length distribution as

$$\pi(t) = \lim_{M \to \infty} \prod_{m=1}^{M} \sum_{i_{m}=1}^{N} \sum_{n_{m}=0}^{\infty} \frac{C_{M}^{(n_{m}, i_{m})}(t)}{\sqrt{N}} P_{n_{m}}(i_{m-1}, i_{m}),$$
(6)

where $C_M^{(n_m,i_m)}(t) \equiv e^{i\Gamma_{i_m}t/M} \left(i\gamma t/M\right)^{n_m}/n_m!$. Note that the probability amplitude can also be related to the path length distribution $P_n(i,j)$ by following the Green's function formalism with the propagator $G_{0i}(\omega) = 1/(\omega - \gamma d_i + \gamma_w \delta_{i,w})$.

We also find a relation between the finding probability P and the optimal hopping parameter γ for the WS model, the Sierpinski carpet, the (extended) fractal- β model with the Sierpinski gasket (Fig. 4). Those data are well fitted by the relation

$$P(\gamma) = \frac{1}{A + (D\gamma + B)^C},\tag{7}$$

with the fitting parameters A = 0.991(1), B = 0.086(5)

and C = 1.68(2). Here, D is fixed as D = 1 for the (extended) fractal- β model and Sierpinski carpet (solid line in Fig. 4), and D is a fitting parameter, the value of which is D = 2.11(1), for the (extended) WS model (dashed line in Fig. 4). In the extended WS model and the extended fractal- β model, which is based on the variant small-world model with shortcuts [5, 83, 84], edges are added randomly with the probability β , which enables us to produce the data sets at $10^{-2} < \gamma < 10^{0}$. In the complete graph, an analytic form of $P(\gamma)$ is known [66], where $P(\gamma = 1/N) \simeq 1$ [59]. The scaling function (7) is also useful not only for the model network, but also for the real-world complex network [85], such as the coauthorship network [80], human disease network [81], and mouse brain network [82] (Fig. 4). We also found other classes of networks that do not show the correlation (7): for example, the Erdös–Rényi random graph, hypercube lattices, fractal Cayley tree [66], T fractal network graph [66], and real-world networks such as dolphin network [86] and Facebook network [87, 88].

In summary, we uncovered the universal perspective of the quantum spatial search in the complex networks. Using the continuous-time quantum walk in the Watts-Strogatz model, the fractal- β model and the static scalefree network model, which covers the regular, random, small-world and scale-free networks, we have demonstrated that as a function of the average path length, the collapse plot can emerge in the finding probability, optimal time, as well as optimal hopping parameter. We also established the explicit relation between the probability amplitude of the target node and the path length distribution by using the path integral formalism. The idea of the complex network science is still useful in the quantum complex network systems, and our results provide a new insight into the connection between quantum physics and complex network science.

ACKNOWLEDGEMENT

S.W. was supported by JST, PRESTO Grant Number JPMJPR211A, Japan. This work was supported by STADHI Satellite Lab, International Research Frontiers Initiative (Institute of Innovative Research, School of Environment and Society), Tokyo Institute of Technology.

- * 1221706@ed.tus.ac.jp
- † watabe@shibaura-it.ac.jp
- [1] A.-L. Barabási and R. Albert, Science 286, 509 (1999).
- [2] D. J. Watts and S. H. Strogatz, nature **393**, 440 (1998).
- [3] C. Song, S. Havlin, and H. A. Makse, Nature **433**, 392 (2005).
- [4] L. A. Amaral and J. M. Ottino, The European physical journal B 38, 147 (2004).

- [5] M. E. Newman, SIAM review 45, 167 (2003).
- [6] R. Albert and A.-L. Barabási, Rev. Mod. Phys. 74, 47 (2002).
- [7] A.-L. Barabási and M. Pósfai, Network science (Cambridge University Press, Cambridge, 2016).
- [8] M. Newman, Networks: An Introduction (Oxford University Press, Inc., USA, 2010).
- [9] J. Biamonte, M. Faccin, and M. D. Domenico, Communications Physics **2**, 1 (2019).
- [10] W. W. Zachary, Journal of Anthropological Research 33, 452 (1977), full publication date: Winter, 1977.
- [11] J. Reichardt and S. Bornholdt, Physical Review Letters 93, 290 (2004).
- [12] A. E. Motter, Physical Review Letters 93, 167 (2004).
- [13] D. Brockmann and D. Helbing, Science 342, 1337 (2013), https://www.science.org/doi/pdf/10.1126/science.1245200.
- [14] S. Perseguers, M. Lewenstein, A. Acín, and J. I. Cirac, Nature Physics 6, 539 (2010).
- [15] X. Guo, C. R. Breum, J. Borregaard, S. Izumi, M. V. Larsen, T. Gehring, M. Christandl, J. S. Neergaard-Nielsen, and U. L. Andersen, Nat Phys 16, 1 (2020).
- [16] J. Rubio, P. A. Knott, T. J. Proctor, and J. A. Dunningham, Journal of Physics A: Mathematical and Theoretical 53, 344001 (2020).
- [17] F. Hahn, A. Pappa, and J. Eisert, npj Quantum Information 5, 1 (2019).
- [18] A. Acín, J. I. Cirac, and M. Lewenstein, Nature Physics 3, 256 (2007).
- [19] M. Cuquet and J. Calsamiglia, Physical Review Letters 103, 240503 (2009).
- [20] H. J. Kimble, Nature 453, 1023 (2008).
- [21] C. Simon, Nature Photonics 11, 678 (2017).
- [22] S. Wehner, D. Elkouss, and R. Hanson, Science 362, eaam9288 (2018).
- [23] S. Brito, A. Canabarro, R. Chaves, and D. Cavalcanti, Phys. Rev. Lett. 124, 210501 (2020).
- [24] P. Erdös and A. Rényi, Publicationes Mathematicae Debrecen 6, 290 (1959).
- [25] M. E. J. Newman, S. H. Strogatz, and D. J. Watts, Physical Review E 64, 290 (2001).
- [26] M. E. Newman and D. J. Watts, Physical review E 60, 7332 (1999).
- [27] L. A. Adamic, R. M. Lukose, A. R. Puniyani, and B. A. Huberman, Physical Review E 64, 651 (2001).
- [28] K. I. Goh, G. Salvi, B. Kahng, and D. Kim, Physical Review Letters 96, 35 (2006).
- [29] S.-H. Yook, F. Radicchi, and H. Meyer-Ortmanns, Phys. Rev. E 72, 045105 (2005).
- [30] N. Masuda and N. Konno, Phys Rev E Stat Nonlin Soft Matter Phys 69, 1568 (2004).
- [31] P. E. Parris and V. M. Kenkre, Phys Rev E Stat Nonlin Soft Matter Phys **72**, 347 (2005).
- [32] S. Hwang, C.-K. Yun, D.-S. Lee, B. Kahng, and D. Kim, Physical Review E 82, 056110 (2010).
- [33] T. J. Perkins, E. Foxall, L. Glass, and R. Edwards, Nature Communications 5, 1 (2019).
- [34] B. Barzel and A.-L. Barabási, Nat Phys 9, 673 (2013).
- [35] M. A. Valdez, D. Jaschke, D. L. Vargas, and L. D. Carr, Phys. Rev. Lett. 119, 225301 (2017).
- [36] M. P. Estarellas, T. Osada, V. M. Bastidas, B. Renoust, K. Sanaka, W. J. Munro, and K. Nemoto, Science Advances 6, eaay8892 (2020), https://www.science.org/doi/pdf/10.1126/sciadv.aay8892.

- [37] L. Jahnke, J. W. Kantelhardt, R. Berkovits, and S. Havlin, Physical Review Letters 101, 1032 (2008).
- [38] R. Bueno and N. Hatano, Phys. Rev. Res. 2, 033185 (2020).
- [39] G. Bianconi and A.-L. Barabási, Physical Review Letters 86, 5632 (2001).
- [40] J. N. Bandyopadhyay and S. Jalan, Phys. Rev. E 76, 026109 (2007).
- [41] F. Radicchi, J. J. Ramasco, A. Barrat, and S. Fortunato, Phys. Rev. Lett. 101, 148701 (2008).
- [42] C. F. A. Negre, H. Ushijima-Mwesigwa, and S. M. Mniszewski, PLOS ONE 15, e0227538 (2020).
- [43] N. Shenvi, J. Kempe, and K. B. Whaley, Physical Review A 67, 052307 (2003).
- [44] M. Faccin, P. Migdał, T. H. Johnson, V. Bergholm, and J. D. Biamonte, Physical Review X 4, 1082 (2014).
- [45] K. Mukai and N. Hatano, Phys. Rev. Res. 2, 023378 (2020).
- [46] S. Dernbach, Applied Network Science 4, 1 (2019).
- [47] J. a. P. Moutinho, A. Melo, B. Coutinho, I. A. Kovács, and Y. Omar, Phys. Rev. A 107, 032605 (2023).
- [48] W. Liang, F. Yan, A. M. Iliyasu, and A. S. Salama, in 2022 IEEE 2nd International Conference on Information Communication and Software Engineering (ICI-CSE) (2022) pp. 1–5.
- [49] E. Sánchez-Burillo, J. Duch, J. Gómez-Gardeñes, and D. Zueco, Sci Rep 2, 1225 (2012), burillo et al.11 rely on a mixture of unitary and dissipative evolution to define a ranking that converges faster than classical Page-Rank.
- [50] J. A. Izaac, J. B. Wang, P. C. Abbott, and X. S. Ma, Phys. Rev. A 96, 032305 (2017).
- [51] Y. Wang, S. Xue, J. Wu, and P. Xu, Scientific Reports 12, 6001 (2022).
- [52] A. M. Childs, E. Farhi, and S. Gutmann, 1, 35 (2002).
- [53] J. D. Whitfield, C. A. Rodríguez-Rosario, and A. Aspuru-Guzik, Physical Review A 81, 856 (2010).
- [54] M. Faccin, T. Johnson, J. Biamonte, S. Kais, and P. Migdał, Physical Review X 3, 452 (2013).
- [55] F. Zähringer, G. Kirchmair, R. Gerritsma, E. Solano, R. Blatt, and C. F. Roos, Physical Review Letters 104, 100503 (2010).
- [56] A. Schreiber, K. N. Cassemiro, V. Potoček, A. Gábris, P. J. Mosley, E. Andersson, I. Jex, and C. Silberhorn, Physical Review Letters 104, 21 (2010).
- [57] L. Xiao, X. Qiu, K. Wang, Z. Bian, X. Zhan, H. Obuse, B. C. Sanders, W. Yi, and P. Xue, Physical Review A 98, 1 (2018).
- [58] M. Karski, L. Förster, J.-M. Choi, A. Steffen, W. Alt, D. Meschede, and A. Widera, Science 325, 174 (2009), https://www.science.org/doi/pdf/10.1126/science.1174436.
- [59] A. M. Childs and J. Goldstone, Phys. Rev. A 70, 022314 (2004).
- [60] A. Patel and M. A. Rahaman, Phys. Rev. A 82, 032330 (2010).
- [61] A. Patel, K. S. Raghunathan, and M. A. Rahaman, Phys. Rev. A 82, 032331 (2010).

- [62] S. Chakraborty, L. Novo, A. Ambainis, and Y. Omar, Physical review letters 116, 100501 (2016).
- [63] A. Glos, A. Krawiec, R. Kukulski, and Z. Puchała, Quantum Information Processing 17, 1 (2018).
- [64] T. Osada, K. Sanaka, W. J. Munro, and K. Nemoto, Physical Review A 97, 1 (2018).
- [65] Z. Darázs, A. Anishchenko, T. Kiss, A. Blumen, and O. Mülken, Phys Rev E Stat Nonlin Soft Matter Phys 90, 032113 (2014).
- [66] E. Agliari, A. Blumen, and O. Muelken, Physical Review A 82, 012305 (2010).
- [67] S. Tamegai, S. Watabe, and T. Nikuni, Journal of the Physical Society of Japan 87, 085003 (2018).
- [68] R. Sato, T. Nikuni, and S. Watabe, Physical Review A 101, 022312 (2020).
- [69] S. Boettcher, S. Li, T. D. Fernandes, and R. Portugal, Phys. Rev. A 98, 012320 (2018).
- [70] A. Patel and K. S. Raghunathan, Phys. Rev. A 86, 012332 (2012).
- [71] D. I. Tsomokos, Phys. Rev. A 83, 052315 (2011).
- [72] T. Osada, B. Coutinho, Y. Omar, K. Sanaka, W. J. Munro, and K. Nemoto, Physical Review A 101, 022310 (2020).
- [73] A.-L. Barabási, Philosophical Transactions of the Royal Society A: Mathematical, Physical and Engineering Sciences 371, 20120375 (2013).
- [74] M. Tomochi, Sociological Theory and Methods 25, 19 (2010).
- [75] K.-I. Goh, B. Kahng, and D. Kim, Phys. Rev. Lett. 87, 278701 (2001).
- [76] M. Boguná and R. Pastor-Satorras, Physical Review E 68, 036112 (2003).
- [77] G. Caldarelli, A. Capocci, P. De Los Rios, and M. A. Munoz, Physical review letters 89, 258702 (2002).
- [78] B. Söderberg, Physical review E 66, 066121 (2002).
- [79] M. E. J. Newman and G. T. Barkema, Monte Carlo methods in statistical physics (Clarendon Press, Oxford, 1999).
- [80] M. E. Newman, Physical Review E 74, 036104 (2006).
- [81] K.-I. Goh, M. E. Cusick, D. Valle, B. Childs, M. Vidal, and A.-L. Barabási, Proceedings of the National Academy of Sciences 104, 8685 (2007).
- [82] K. Amunts, C. Lepage, L. Borgeat, H. Mohlberg, T. Dickscheid, M.-É. Rousseau, S. Bludau, P.-L. Bazin, L. B. Lewis, A.-M. Oros-Peusquens, N. J. Shah, T. Lippert, K. Zilles, and A. C. Evans, Science 340, 1472 (2013).
- [83] R. Monasson, The European Physical Journal B Condensed Matter and Complex Systems 12, 555 (1999).
- [84] M. Newman and D. Watts, Physics Letters A 263, 341 (1999).
- [85] R. Rossi and N. Ahmed, Proceedings of the AAAI Conference on Artificial Intelligence 29 (2015).
- [86] D. Lusseau, Evolutionary ecology 21, 357 (2007).
- [87] A. L. Traud, E. D. Kelsic, P. J. Mucha, and M. A. Porter, SIAM Rev. 53, 526 (2011).
- [88] A. L. Traud, P. J. Mucha, and M. A. Porter, Phys. A 391, 4165 (2012).

Supplemental Materials for "Universal scaling laws of quantum spatial search in complex networks"

Rei Sato, ^{1, 2, *} Tetsuro Nikuni, ¹ Kayoko Nohara, ² Giorgio Salani, ² and Shohei Watabe ^{1, 3, †}

¹ Department of Physics, Tokyo University of Science, Shinjuku, Tokyo, 162-8601, Japan

² Department of Transdisciplinary Science and Engineering,
School of Environment and Society, Tokyo Institute of Technology,

²⁻¹²⁻¹ O-okayama, Meguro-ku, Tokyo 152-8550, Japan

³ Faculty of Engineering, Computer Science and Engineering,
Shibaura Institute of Technology, Toyosu, Tokyo, 135-8548, Japan

Appendix A: Network Structure

In this section, we summarize the complex network models used in this paper. For the small-world network, we employ the Watts-Strogatz (WS) model [1], the fractal- β model [2], which can cover not only the small-world network but also the regular ring, the regular fractal and random graphs. The method to generate a small-world network is proposed by Watts and Strogatz [1], which is based on a ring graph, but can be extended to other regular networks, such as a square, triangle and fractal lattices [2]. For example, starting with a regular ring network of N-vertices with the degree k, each node is randomly rewired with a probability β . By changing the probability from $\beta = 0$ to $\beta = 1$, this model interpolates the small-world network from the regular to random networks. For $\beta = 0$, no edges are rewired, where the network keeps the original regular graph. For $\beta = 1$, all the edges are randomly rewired, which results in a random network. A local clustering coefficient C_i , which is used in the average clustering coefficient $C = \sum_{i=1}^{N} C_i/N$, is defined as $C_i = \Delta_i/(k_i C_2)$ for a node i with a degree k_i , and Δ_i represents the number of edges between k_i -neighbor nodes.

For the scale-free network, we utilize the static scale-free network model [3], because the number of nodes N can be easily managed and constant through the network generation process rather than the growing network model, or the Barabási-Albert model [4]. To generate a scale-free network with a degree exponent λ , the following algorithm is used [3]; Each vertex is indexed by an integer i for $i=1,\cdots,N$. A probability $p_i=i^{-\alpha}/\sum_{j=1}^N j^{-\alpha}$ is assigned to each vertex with a parameter $\alpha \in [0,1]$. Two different vertices i and j are randomly selected with probabilities p_i and p_j , respectively, and if there are no links between them, a link is created. This process is stopped if the number of generated edges reaches a value mN with a constant m, where the mean degree is given by $\langle k \rangle = 2m$. The exponent λ in the degree distribution $P_k \sim k^{-\lambda}$ in this model can be related to the parameter α , given by $\lambda = 1 + 1/\alpha$ [3]. By controlling the parameter $\alpha \in [0,1]$, therefore, we can generate the networks with the degree distribution for

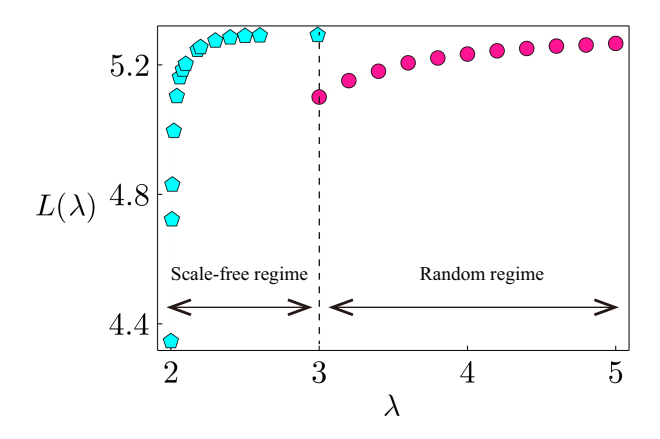


Figure 1. (Color online) The λ -dependence of the average path length L in the static scale-free model, where λ is an exponent of the degree distribution, given by $P_k \sim k^{-\lambda}$.

^{* 1221706@}ed.tus.ac.jp

[†] watabe@shibaura-it.ac.jp

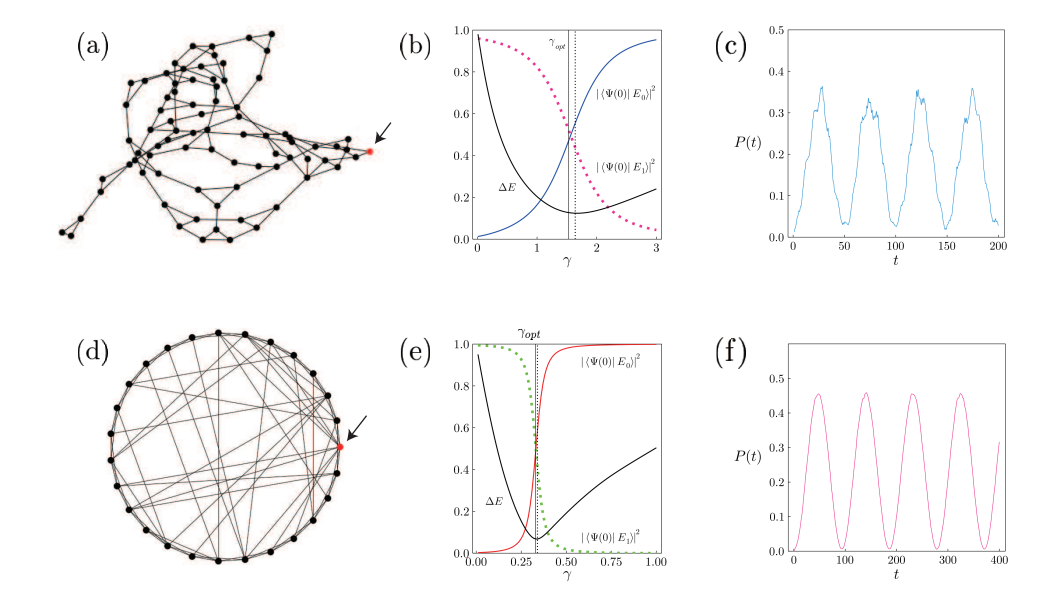


Figure 2. (Color online) (a-c) Fractal- β model for $\beta=0.2$ and $N=3^4$ at the stage S=4, where the regular network at $\beta=0$ is the Sierpinski gasket. (d-f) The WS model for $\beta=0.6$. (a) A network of a fractal- β model, where the red point pointed by arrow is a target site w. (b) Energy gap ΔE and overlaps $|\langle \Psi(0)|E_{0,1}\rangle|^2$ for the fractal- β model. The dotted vertical line indicates γ for the minimum energy gap. The solid vertical line at $\gamma=1.53$ is the position where $|\langle \Psi(0)|E_0\rangle|^2=|\langle \Psi(0)|E_1\rangle|^2\simeq 0.5$ holds. (c) Time-dependence of the finding probability P(t) at a target site w with $\gamma=1.53$. (d) A network of the WS model for N=27. (e) Energy gap and overlaps for the WS model with N=400. The dotted vertical line indicates γ for the minimum energy gap. The solid vertical line at $\gamma=0.33$ is the position where $|\langle \Psi(0)|E_0\rangle|^2=|\langle \Psi(0)|E_1\rangle|^2\simeq 0.5$ holds. (f) Time-dependence of the finding probability P(t) at a target site w with $\gamma=0.33$ and N=400.

 $2 \le \lambda$ [3]. For $\lambda < 2$, the network is in an anomalous regime, where the average path length does not depend on N. For $2 < \lambda < 3$, the network is in the scale-free regime with an ultra-small world property, where $L \sim \ln \ln N$. For $\lambda > 3$, the network is in the random regime with a small-world property, where $L \sim \ln N$. The critical points emerge at $\lambda = 2$ with L = const. and at $\lambda = 3$ with $L = \ln N / \ln \ln N$ (Fig. 1).

Appendix B: Quantum Spatial Search

The quantum spatial search for a target node w using the continuous-time quantum walk is achieved by using the Schrödinger equation

$$i\frac{d}{dt}|\Psi(t)\rangle = \hat{H}|\Psi(t)\rangle,$$
 (B1)

where the time-independent Hamiltonian $\hat{H} = \hat{H}_L + \hat{H}_w$ is given by

$$\hat{H}_L = \gamma \hat{L},\tag{B2}$$

$$\hat{H}_w = -\gamma_w |w\rangle\langle w|. \tag{B3}$$

Here, $\gamma(>0)$ is a hopping parameter, and $\gamma_w(>0)$ is the strength of the target potential, which is often normalized as $\gamma_w = 1$. The Laplacian operator \hat{L} is given by

$$\hat{L} = \sum_{ij} L_{ij} |i\rangle\langle j| \equiv \hat{D} - \hat{A},\tag{B4}$$

where the operators \hat{D} and \hat{A} are the degree and adjacency operators, respectively, given by

$$\hat{D} = \sum_{ij} D_{ij} |i\rangle\langle j|, \quad \hat{A} = \sum_{ij} A_{ij} |i\rangle\langle j|.$$
(B5)

\overline{t}	$10^4 \sim 10^6$
β	$0, 2.5 \times 10^{-3}, 7 \times 10^{-3}, 0.02, 0.04, 0.08, 0.2, 0.4, 0.6, 1$
λ (scale-free)	2.0, 2.007, 2.01, 2.02, 2.08, 2.99
λ (random)	3.0, 3.2, 3.4, 3.6, 3.8, 4.0, 4.2, 4.4

Table I. Parameter sets we used to find the collapse plot. β is for the WS model and the fractal- β model. λ is for the static scale-free model.

Here, $D_{ij} \equiv d_i \delta_{ij}$ gives the degree matrix with the degree d_i for the node i, and A_{ij} is the adjacency matrix of the graph G we are interested in, given by

$$A_{ij} = \begin{cases} 1 & (i,j) \in G, \\ 0 & \text{otherwise.} \end{cases}$$
 (B6a)

After generating networks such as the fractal- β model (Fig. 2 (a)) and the WS model (Fig. 2 (d)), we optimize the hopping parameter γ , to estimate which we can choose two possible conditions [5]. The condition (i) is that the overlap between the ground state $|E_0\rangle$ of \hat{H} and the initial equal-superposition state $|s\rangle$ is equal to that for the first-excited state $|E_1\rangle$, which is close to 0.5, i.e., $|\langle s|E_0\rangle|^2 = |\langle s|E_1\rangle|^2 \simeq 0.5$. The condition (ii) is that the energy gap ΔE between the first-excited and ground states is minimum. The earlier study [5] reported that the values of γ in the conditions (i) and (ii) are almost equal.

Both in the fractal- β model (Fig. 2 (b)) and the WS model (Fig. 2 (e)), however, we found a small but significant difference between the values of γ satisfying the overlap condition (i) and the minimum-energy-gap condition (ii). By comparing the finding probability $P(t) = |\langle w| e^{-i\hat{H}t} |s\rangle|^2$ on a target node w for two different values of γ , the higher peak and clearer periodicity emerge in the condition (i) rather than (ii) (Figs. 2 (c) and (f)). We thus estimate the optimal value γ by using the condition (i).

Appendix C: Numerical results and data analysis

In order to analyze the scaling law, we perform numerical simulations, where the simulation time is ranging from t = 10000 to 1000000. The parameter sets for simulations are summarized in Table I. We randomly generate networks by changing probabilities β and λ .

We determine the optimal value of the hopping parameter γ , the condition of which is given by $|\langle E_0|s\rangle| = |\langle E_1|s\rangle|$. Using the finding probability $P(\omega)$ in the frequency space after the Fourier transformation of P(t), we extract the optimal frequency ω from the maximum value of $P(\omega)$, which determines the optimal time Q that gives the peak-to-peak period of the finding probability. Using this optimal time Q, we gather the peak values of P(t) in a long-time Schrödinger-dynamics simulation., which produces the average finding probability P.

In the following, we explain the process of trial-and-error to find the collapse plot for the quantum spatial search in the complex network. We first analyzed the conventional scaling law for the fractal- β and WS models as a function of the number of sites N, supposing the relation $\gamma(\beta) = \mathcal{O}(N^{a_{\gamma}})$, $Q(\beta) = \mathcal{O}(N^{a_{Q}})$ and $P(\beta) = \mathcal{O}(N^{a_{P}})$ (Figs. 3 (a)-(c) and (g)-(i)). However, we could not find characteristic universal behaviors in the WS model and fractal- β model for various values of β .

Since the path length is a key quantity in the complex network, we tried to plot the data as a function of the average path length $L(\beta)$ (Figs. 3 (d)-(f) and (j)-(l)). However, the simple plot as a function of the average path length $L(\beta)$ is also not useful to show the characteristic behavior, where the average path lengths spread in different orders. Therefore, the normalization of the path length is important for networks with the same number of nodes N with different β , such as $L(\beta)/L(0)$.

For the fractal- β model, we analyze the data by supposing the relation $\gamma(\beta) = D_{\gamma} (L(\beta)/L(0))^{\alpha_{\gamma}}$, $Q(\beta) = D_{Q} (L(\beta)/L(0))^{\alpha_{Q}}$ and $P(\beta) = D_{P} (L(\beta)/L(0))^{\alpha_{P}}$ (Figs. 4 (a), (d),(g)). Surprisingly, we find the universal exponent $\alpha_{\gamma,Q,P}$ for the normalized average path length $L(\beta)/L(0)$. We analyze the coefficients $D_{\gamma,Q,P}$ and the exponents $\alpha_{\gamma,Q,P}$ as a function of N in the fractal- β model (Figs. 4 (d)-(i)), which gives

$$D_{\gamma} = 0.299(9)N^{0.485(3)}, \quad \alpha_{\gamma} = 1.04(3) + 2.7(9)N^{-0.46(9)},$$
 (C1)

$$D_Q = 0.81(4)N^{0.989(6)}, \quad \alpha_Q = 0.94(1) + 0(2)N^{-0.6(8)},$$
 (C2)

$$D_P = 10.8(5)N^{-0.908(9)}, \quad \alpha_P = -1.82(3) + 3.1(8)N^{-0.54(7)}.$$
 (C3)

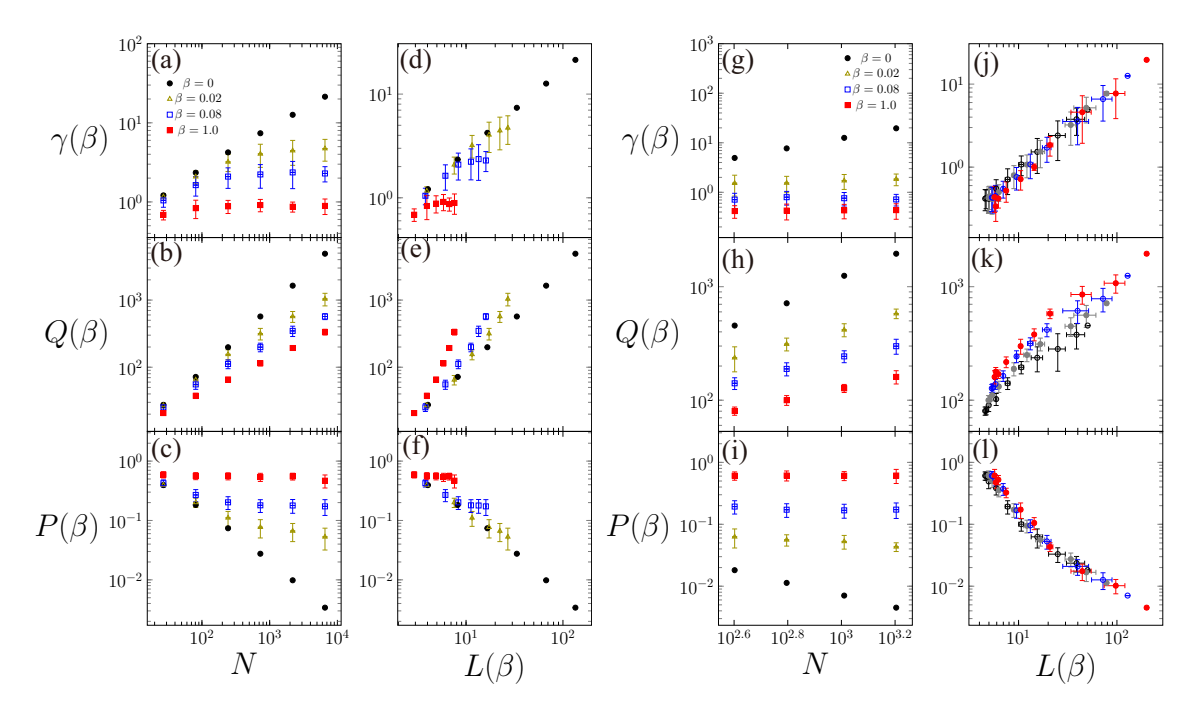


Figure 3. (Color online) Quantum spatial search in the small-wold network. (a-f) The fractal- β model for the stage S=3-8, where the regular lattice at $\beta=0$ is the Sierpinski gasket. (g-i) The WS model with N=400, 625, 1024, 1600. Here, we plot the data as a function of the number of nodes N [(a)-(c), (g)-(i)], and as a function of the average path length $L(\beta)$ [(d)-(f), (j)-(l)]. The mean values of the optimal hopping parameter γ [(a), (d), (g), (j)], the optimal time Q [(b), (e), (h), (k)], and the maximum finding probability P at a target site [(c), (f), (i), (l)].

D_{γ}	D_Q	D_P	$\gamma(0)$	Q(0)	P(0)
u 0.299(9)	0.81(4)	10.8(5)	0.299(9)	0.81(4)	10.8(5)
b 0.485(3)	0.989(6)	-0.908(9)	0.485(3)	0.989(6)	-0.908(9)

Table II. Scaling factors of D_{γ} , D_{Q} , D_{P} and $\gamma(0)$, Q(0), P(0) in the fractal- β model, where excellent agreements can be found. We assume the scaling laws uN^{b} , where all fittings are performed from S = 5 to 8.

We found that the scaling of the coefficients $D_{\gamma,Q,P}$ are excellently the same as that in the regular fractal network for $\beta = 0$ (Fig. 5 and Table II), i.e.,

$$D_{\gamma} = \gamma(0), \quad D_{Q} = Q(0), \quad D_{P} = P(0).$$
 (C4)

As a result, we have the scaling relations

$$\frac{\gamma(\beta)}{\gamma(0)} = \left(\frac{L(\beta)}{L(0)}\right)^{\alpha_{\gamma}}, \quad \frac{Q(\beta)}{Q(0)} = \left(\frac{L(\beta)}{L(0)}\right)^{\alpha_{Q}}, \quad \frac{P(\beta)}{P(0)} = \left(\frac{L(\beta)}{L(0)}\right)^{\alpha_{P}}. \tag{C5}$$

In the large-N limit, the exponents converge as $\alpha_{\gamma} = 1.04(3)$, $\alpha_{P} = 0.94(1)$ and $\alpha_{Q} = -1.82(3)$, respectively. We can also successfully make the collapse plot in the WS model. Away from the regime for the regular network ($\beta = 0$), or $L(\beta)/L(0) = 1$, the exponents for the WS model and the fractal- β model are equivalent, the average values of which are given by

$$\alpha_{\gamma} = 1.08(6), \quad \alpha_{Q} = 0.90(5), \quad \alpha_{P} = -1.76(8).$$
 (C6)

We tried to make plots as a function of the average cluster coefficient $C(\beta)$ as well as the normalized average cluster coefficient $C(\beta)/C(0)$. However, we could not make any collapse plots of γ , Q and P for the (normalized) average cluster coefficients. In short, the scaling law on a small-world network is found to be determined by the average path length.

We also confirmed that the collapse plots can be found in the scale-free networks for the normalized average path

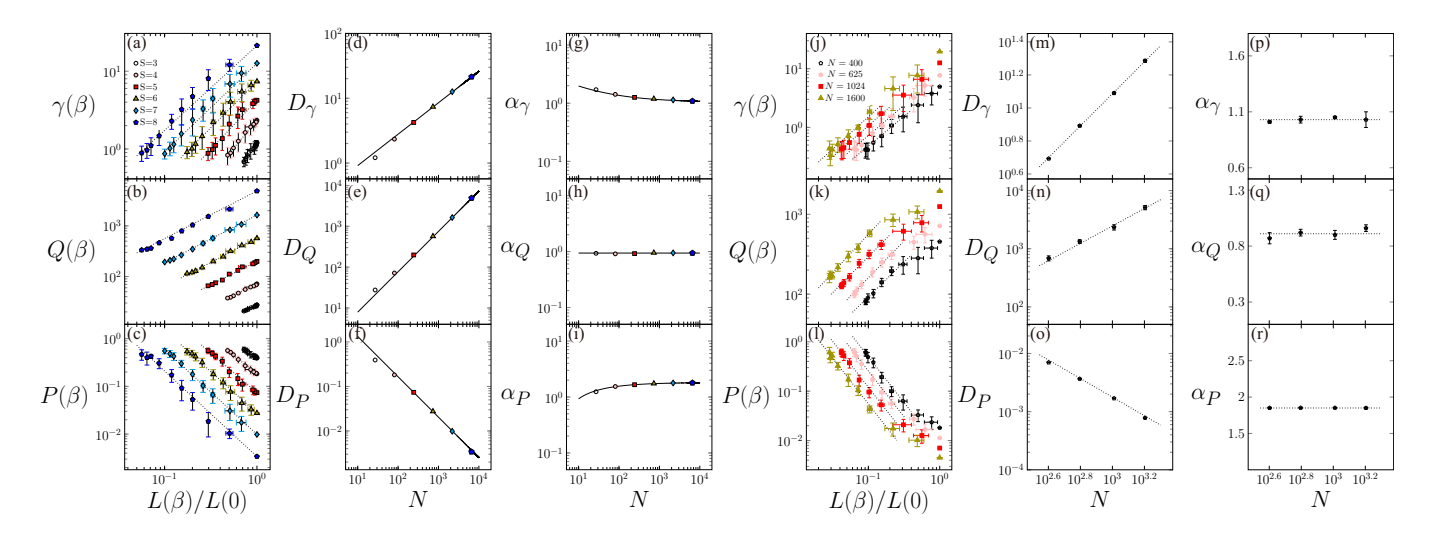


Figure 4. (Color online) Scaling laws for the small-world network in the fractal- β model (a)-(i) and in the WS model (j)-(r). γ , Q and P as a function of the normalized average path length $L(\beta)/L(0)$ [(a)-(c), (j)-(l)]. The dashed line is the fitting with $\gamma = D_{\gamma} (L(\beta)/L(0))^{\alpha_{\gamma}}$, $Q = D_{Q} (L(\beta)/L(0))^{\alpha_{Q}}$, $P = D_{P} (L(\beta)/L(0))^{\alpha_{P}}$, respectively. The scaling of the coefficients D_{γ} , D_{Q} and D_{P} as a function of the number of sites N with the fitting form uN^{b} [(d)-(f), (m)-(o)]. The exponents α_{γ} , α_{Q} , α_{P} as a function of N with the fitting form $p + qN^{r}$ [(g)-(i), (p)-(r)]. All fittings are performed for the stages S = 5-8 in the fractal- β model.

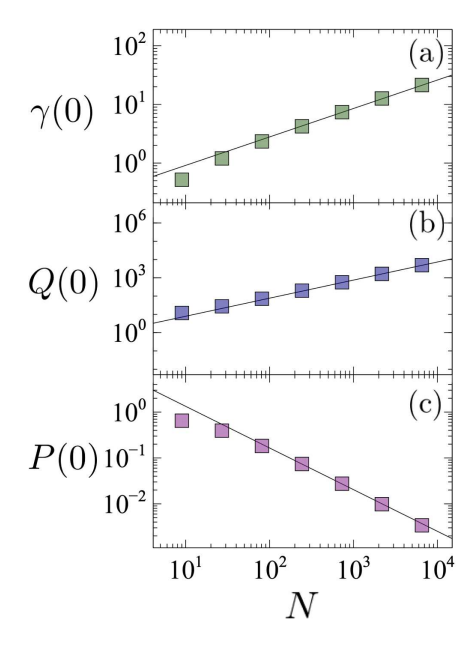


Figure 5. (Color online) Quantum spatial search on Sierpinski gaskets from S=2 to 8, which corresponds to the fractal- β model for $\beta=0$. (a) The hopping parameter γ , (b) the optimal time Q and (c) the finding probability P. Lines are fittings with the form uN^b . All fittings are performed from S=5 to 8.

length. First of all, any characteristic universal behaviors cannot be found in the the N-dependence of γ , Q and P (Fig. 6). In the simulation for the static scale-free model, we used $\lambda = \{2, 2.007, 2.01, 2.02, 2.08, 2.99\}$ for the scale-free regime with $N = \{800, 1024, 2500\}$, and $\lambda = \{3, 3.2, 3.4, 3.6, 3.8, 4, 4.2, 4.4\}$ for the random regime with $N = \{800, 1024, 2500\}$. We selected a target as a node with the minimum degree k_{\min} [Figs. 6 (a)-(c), (j)-(l)], a node with the median degree k_{\max} [Figs. 6 (g)-(i), (p)-(r)].

For normalized quantities $\gamma(\lambda)/\gamma(\lambda_0)$, $Q(\lambda)/Q(\lambda_0)$ and $P(\lambda)/P(\lambda_0)$, the collapse plots can be excellently organized as a function of the normalized average path length $L(\lambda)/L(\lambda_0)$, where data for different sizes of networks are well integrated into single curves (Fig. 7). As a reference, we chose $\lambda_0 = 2$ for the scale-free regime $(2 < \lambda < 3)$ and $\lambda_0 = 4.5$

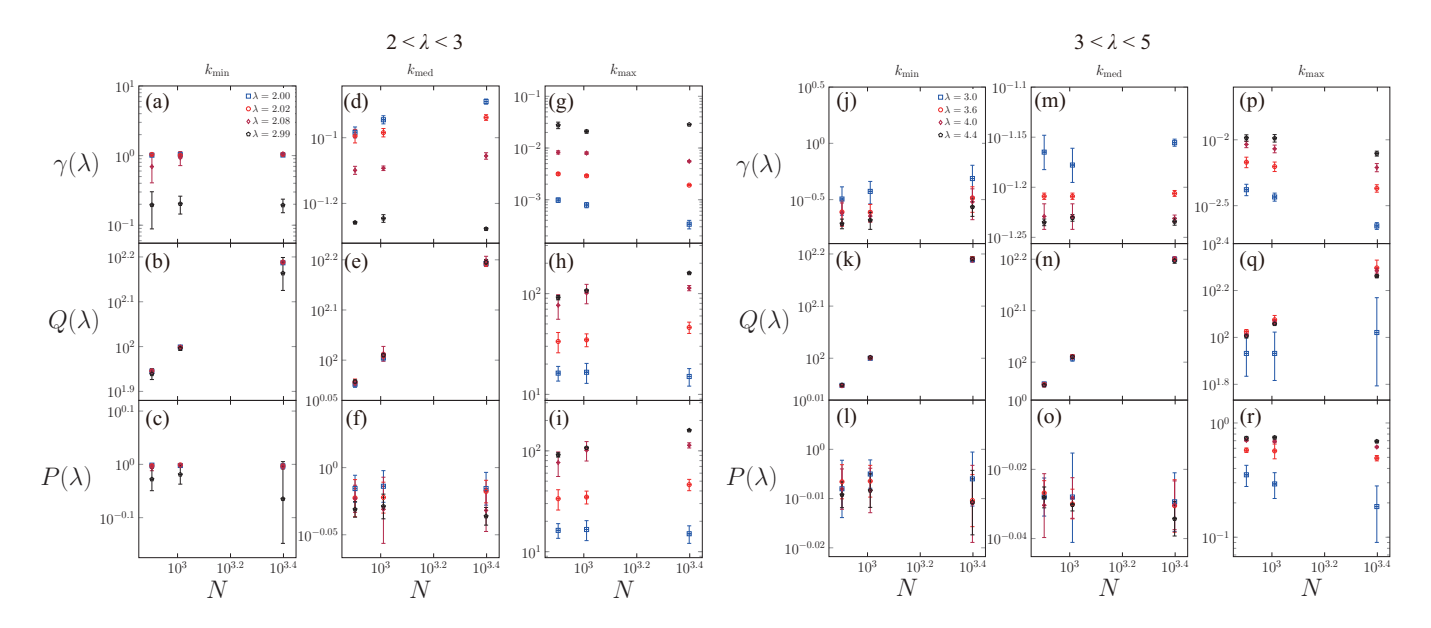


Figure 6. (Color online) Quantum spatial search in the static scale-free model for the scale-free regime with the ultra-small world property (a)-(i) and for the random regime with the small-world property (j)-(r). The mean values of the optimal hopping parameter γ [(a), (d), (g), (j), (m), (p)], the optimal time Q [(b), (e), (h), (k), (n), (q)] and the maximum finding probability P [(c), (f), (i), (l), (o), (r)] as a function of the number of nodes N. The target is selected as a node with the minimum degree k_{\min} [(a)-(c), (j)-(l)], with the median degree k_{\max} [(d)-(f), (m)-(o)] and with the maximum degree k_{\max} , the node with which is a hub [(g)-(i), (p)-(r)].

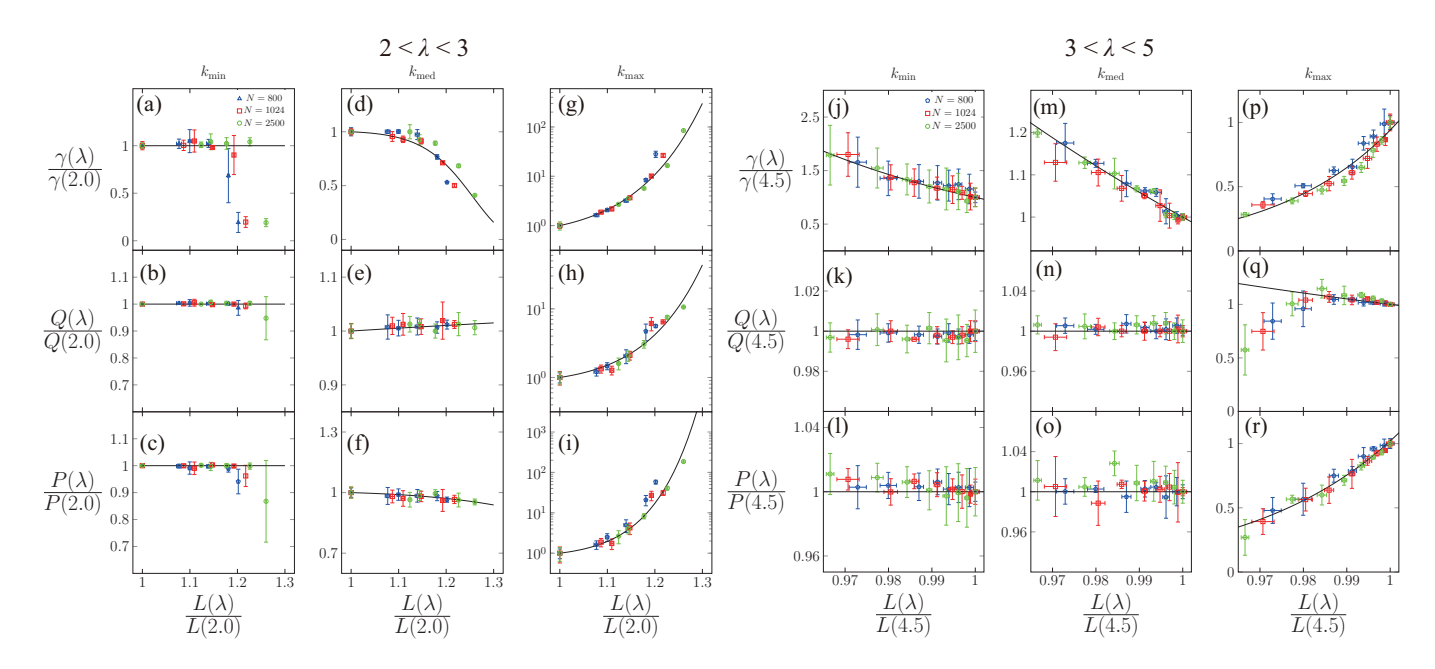


Figure 7. Collapse plots of data in Fig. 6 for the scale-free regime with the ultra-small world property (a)-(i) and for the random regime with the small-world property (j)-(r). The mean values of the normalized optimal hopping parameter $\gamma(\lambda)/\gamma(\lambda_0)$ [(a), (d), (g), (j), (m), (p)], the normalized optimal time $Q(\lambda)/Q(\lambda_0)$ [(b), (e), (h), (k), (n), (q)] and the normalized maximum finding probability $P(\lambda)/P(\lambda_0)$ [(c), (f), (i), (l), (o), (r)] as a function of the normalized average path length $L(\lambda)/L(\lambda_0)$. We chose $\lambda_0 = 2$ for $2 < \lambda < 3$ and $\lambda_0 = 4.5$ for $3 < \lambda$ as a reference. The target is selected as a node with the minimum degree k_{\min} [(a)-(c), (j)-(l)], with the median degree k_{\max} [(d)-(f), (m)-(o)] and with the maximum degree k_{\max} , the node with which is a hub [(g)-(i), (p)-(r)]. The solid lines are fittings with the forms summarized in Table III.

	k_{\min}	$k_{ m med}$	$k_{ m max}$
$\gamma(\lambda)/\gamma(2)$	1	$\exp(-0.01(x^{19.9} - 1))$	$0.94(2)x^{37(2)}$
$Q(\lambda)/Q(2)$	1	$\exp(0.31(x^{0.18} - 1))$	$1.00(1)x^{-5(1)}$
$P(\lambda)/P(2)$	1 e	$xp(-0.0091(x^{7.9} - 1))$	$1.02(1)x^{30(1)}$
$\gamma(\lambda)/\gamma(4.5)$ exp	$p(-15(x^{1.19} - 1))$	$\exp(-10(x^{0.57}-1))$	$\exp\left(4.4(4)(x^{9(1)}-1)\right)$
$Q(\lambda)/Q(4.5)$	0.99813	1.002463	$\exp\left(-0.00019(7)(x^{-232(11)}-1)\right)$
$P(\lambda)/P(4.5)$	1.00357	1.003576	$\exp\left(29(7)(x^{0.9(2)}-1)\right)$

Table III. Possible fittings for the collapse plots in the scale-free network shown in Fig. 7, where $x \equiv L(\lambda)/L(\lambda_0)$ with $\lambda_0 = 2$ for the scale-free regime (upper rows) and $\lambda_0 = 4.5$ for the random regime (lower rows), respectively. In the upper rows for k_{\min} , we assumed the data as unity to ignore strong-fluctuation effects emerging around $\lambda = 3$.

for the random regime $(3 < \lambda)$. The fitting functions we used are summarized in TABLE III. As the parameter λ approaches to $\lambda_0 = 3$ from below, strong fluctuations emerge (Figs. 6 (a)-(c)). Interestingly, a hub provides the clear path-length dependence for $\gamma(\lambda)/\gamma(\lambda_0)$, $Q(\lambda)/Q(\lambda_0)$ and $P(\lambda)/P(\lambda_0)$ (Figs. 6 (g)-(i), (p)-(r)). On the other hand, the normalized optimal time $Q(\lambda)/Q(\lambda_0)$ and the normalized finding probability $P(\lambda)/P(\lambda_0)$ do not show the clear path-length dependence and are almost constant for targets with the minimum degree k_{\min} (Figs. 6 (b), (c), (k), (l)), and with the median degree k_{\max} (Figs. 6 (e), (f), (n), (o)).

Appendix D: Relation between the finding probability and the path length distribution

1. Path integral approach

In this section, we explicitly derive the relation between the finding probability and the path length distribution. The finding probability of the quantum spatial search for a target site $|w\rangle$ is given by $|\pi(w,t)|^2$ with the probability amplitude $\pi(w,t) = \langle w|e^{-i\hat{H}t}|s\rangle$, where $|s\rangle$ is the equal-weight superposition state $|s\rangle = \sum_i |i\rangle/\sqrt{N}$ with the number of nodes N. Here $|i\rangle$ is the basis given for the node $i=1,\cdots,N$.

We divide the Hamiltonian $H = \hat{H}_L + \hat{H}_w$ as $H \equiv \hat{H}_A + \hat{H}_d$, given by

$$\hat{H}_A \equiv \hat{H}_L - \gamma \hat{D} = -\gamma \hat{A},\tag{D1}$$

$$\hat{H}_{\rm d} \equiv \hat{H}_w + \gamma \hat{D} = -\sum_i \Gamma_i |i\rangle\langle i|, \tag{D2}$$

where $\Gamma_i = \gamma_w \delta_{i,w} - \gamma d_i$ and \hat{A} is the adjacency operator. By using the Suzuki-Trotterization with the closure relation

 $\sum_{i}|i\rangle\langle i|=\hat{I}$, the probability amplitude $\pi(w,t)=\langle w|e^{-i\hat{H}t}|s\rangle$ is given by

$$\pi(w,t) \equiv \langle w|e^{-i\hat{H}t}|s\rangle \tag{D3}$$

$$= \lim_{M \to \infty} \langle w | (e^{-i\hat{H}_A t/M} e^{-i\hat{H}_d t/M})^M | s \rangle.$$
 (D4)

$$= \lim_{M \to \infty} \langle w | e^{-i\hat{H}_A t/M} e^{-i\hat{H}_d t/M} \left(\sum_{i_1=1}^N |i_1\rangle \langle i_1| \right) e^{-i\hat{H}_A t/M} e^{-i\hat{H}_d t/M} \left(\sum_{i_2=1}^N |i_2\rangle \langle i_2| \right)$$
(D5)

$$\cdots \left(\sum_{i_{M-1}=1}^{N} |i_{M-1}\rangle\langle i_{M-1}|\right) e^{-i\hat{H}_A t/M} e^{-i\hat{H}_d t/M} \left(\sum_{i_{M}=1}^{N} |i_{M}\rangle\langle i_{M}|\right) |s\rangle$$
 (D6)

$$= \lim_{M \to \infty} \sum_{i_1=1}^{N} \langle w | e^{-i\hat{H}_A t/M} e^{-i\hat{H}_{d} t/M} | i_1 \rangle \cdot \sum_{i_2=1}^{N} \langle i_1 | e^{-i\hat{H}_A t/M} e^{-i\hat{H}_{d} t/M} | i_2 \rangle$$
 (D7)

$$\cdots \sum_{i_M=1}^{N} \langle i_{M-1} | e^{-i\hat{H}_A t/M} e^{-i\hat{H}_d t/M} | i_M \rangle \left(\frac{1}{\sqrt{N}} \sum_{j=1}^{N} \langle i_M | j \rangle \right)$$
 (D8)

$$= \frac{1}{\sqrt{N}} \lim_{M \to \infty} \prod_{m=1}^{M} \left[\sum_{i_m=1}^{N} \mathcal{K}_M(i_{m-1}, i_m; t) \right], \tag{D9}$$

where $|i_0\rangle \equiv |w\rangle$ and the kernel is given by $\mathcal{K}_M(i,j;t) \equiv \langle i|e^{-i\hat{H}_At/M}e^{-i\hat{H}_dt/M}|j\rangle$.

The kernel $\mathcal{K}_M(i,j;t)$ can be represented by using the path length distribution. Indeed, the kernel is reduced into

$$\mathcal{K}_M(i,j;t) = \langle i|e^{-i\hat{H}_A t/M} e^{-i\hat{H}_d t/M}|j\rangle \tag{D10}$$

$$= \langle i|e^{-i\hat{H}_A t/M} \sum_{n=0}^{\infty} \frac{1}{n!} \left(\frac{-it}{M}\right)^n \hat{H}_{\mathrm{d}}^n |j\rangle$$
 (D11)

$$= \langle i|e^{-i\hat{H}_A t/M} \sum_{n=0}^{\infty} \frac{1}{n!} \left(\frac{-it}{M}\right)^n \left(-\sum_k \Gamma_k |k\rangle \langle k|\right)^n |j\rangle$$
 (D12)

$$= \langle i|e^{-i\hat{H}_A t/M} \sum_{n=0}^{\infty} \frac{1}{n!} \left(\frac{it}{M}\right)^n \left(\sum_k \Gamma_k^n |k\rangle\langle k|\right) |j\rangle$$
 (D13)

$$= \sum_{n=0}^{\infty} \frac{1}{n!} \left(\frac{i\Gamma_j t}{M} \right)^n \langle i | e^{-i\hat{H}_A t/M} | j \rangle$$
 (D14)

$$=e^{i\Gamma_j t/M} \langle i|e^{-i\hat{H}_A t/M}|j\rangle. \tag{D15}$$

The propagator $\langle i|e^{-i\hat{H}_At/M}|j\rangle$ can be also reduced into

$$\langle i|e^{-i\hat{H}_A t/M}|j\rangle = \langle i|\sum_{n=0}^{\infty} \frac{1}{n!} \left(-\frac{it}{M}\right)^n \hat{H}_A^n|j\rangle \tag{D16}$$

$$= \sum_{n=0}^{\infty} \frac{1}{n!} \left(\frac{i\gamma t}{M} \right)^n \langle i|\hat{A}^n|j\rangle. \tag{D17}$$

Here, the path length distribution $P_n(i,j)$, which gives the number of the paths from the node j to i with the path length n, can be defined by using the adjacency matrix \hat{A} [6], given by

$$P_n(i,j) \equiv \langle i|\hat{A}^n|j\rangle. \tag{D18}$$

As a result, the kernel can be represented by the path length distribution as

$$\mathcal{K}_{M}(i,j;t) = e^{i\Gamma_{j}t/M} \sum_{n=0}^{\infty} \frac{1}{n!} \left(\frac{i\gamma t}{M}\right)^{n} P_{n}(i,j), \tag{D19}$$

and the probability amplitude is thus given by

$$\pi(t) = \frac{1}{\sqrt{N}} \lim_{M \to \infty} \prod_{m=1}^{M} \left[\sum_{i_{m}=1}^{N} \sum_{n_{m}=0}^{\infty} \frac{1}{n_{m}!} \left(\frac{i\gamma t}{M} \right)^{n_{m}} e^{i\Gamma_{i_{m}} t/M} P_{n_{m}}(i_{m-1}, i_{m}) \right]. \tag{D20}$$

2. Green's function approach

The probability amplitude $\pi(w,t)$ is also represented by the Green's function. Here, we introduce the operator

$$i\hat{G}(t,t') = e^{-i\hat{H}(t-t')}\theta(t-t'),$$
 (D21)

which gives $iG_{ij}(t,t') = \langle i|\hat{G}(t,t')|j\rangle$. For t>0, the finding probability amplitude is given by

$$\pi(w,t) = \langle w|e^{-i\hat{H}t}|s\rangle = i\langle w|\hat{G}(t)|s\rangle = i\frac{1}{\sqrt{N}}\sum_{i}G_{wi}(t).$$
 (D22)

Since the equation for $\hat{G}(t)$ is given by

$$i\frac{d}{dt}\hat{G}(t) = \hat{H}\hat{G}(t) + \delta(t)\hat{1},\tag{D23}$$

the equation for $G_{ij}(t)$ is reduced into

$$i\frac{d}{dt}G_{ij}(t) = \langle i|i\frac{d}{dt}\hat{G}(t)|j\rangle = \langle i|\hat{H}\hat{G}(t')|j\rangle + \delta_{ij}\delta(t), \tag{D24}$$

which can be given by the matrix representation as

$$i\frac{d}{dt}\mathbf{G}(t) = \mathbf{H}\mathbf{G}(t) + \mathbf{I}\delta(t),\tag{D25}$$

where **G** and **H** are matrices the element of which are given by G_{ij} and H_{ij} , respectively. Here, **I** is the identity. By using the Fourier transformation

$$\mathbf{G}(t) = \int \frac{d\omega}{2\pi} e^{-i\omega t} \mathbf{G}(\omega), \quad \mathbf{G}(\omega) = \int dt \, e^{i\omega t} \mathbf{G}(t), \tag{D26}$$

we have the following equation

$$\int \frac{d\omega}{2\pi} \omega \mathbf{G}(\omega) e^{-i\omega t} = \int \frac{d\omega}{2\pi} \mathbf{H} \mathbf{G}(\omega) e^{-i\omega t} + \mathbf{I} \int \frac{d\omega}{2\pi} e^{-i\omega t}, \tag{D27}$$

which gives $\omega \mathbf{G}(\omega) = \mathbf{H}\mathbf{G}(\omega) + \mathbf{I}$. As a result, we obtain

$$\mathbf{G}(\omega) = (\omega \mathbf{I} - \mathbf{H})^{-1},\tag{D28}$$

where $\mathbf{H} = \gamma \mathbf{L} + \mathbf{H}_w = \gamma \mathbf{D} - \gamma \mathbf{A} + \mathbf{H}_w$, with $H_{wij} = -\gamma_w \delta_{ij} \delta_{iw}$. The Green's function is now given by

$$\mathbf{G}(\omega) = (\omega \mathbf{I} - \mathbf{H}_w - \gamma \mathbf{D} + \gamma \mathbf{A})^{-1}$$
(D29)

$$= [\mathbf{I} - \gamma \mathbf{G}_0(\omega) \mathbf{A}]^{-1} \mathbf{G}_0(\omega), \tag{D30}$$

where the non-perturbative Green's function

$$\mathbf{G}_0(\omega) = (\omega \mathbf{I} - \mathbf{H}_w - \gamma \mathbf{D})^{-1} \tag{D31}$$

is the diagonal matrix, the element of which is given by

$$G_{0i}(\omega) \equiv G_{0ii}(\omega) = \frac{1}{\omega - \gamma d_i + \gamma_w \delta_{i,w}}.$$
 (D32)

By expanding the term $[\mathbf{I} - \gamma \mathbf{G}_0(\omega) \mathbf{A}]^{-1}$, the Green's function is given by

$$\mathbf{G}(\omega) = \mathbf{G}_0(\omega) + \gamma \mathbf{G}_0(\omega) \mathbf{A} \mathbf{G}_0(\omega) + \gamma^2 \mathbf{G}_0(\omega) \mathbf{A} \mathbf{G}_0(\omega) + \cdots$$
(D33)

$$= \sum_{n=0}^{\infty} [\gamma \mathbf{G}_0(\omega) \mathbf{A}]^n \mathbf{G}_0(\omega). \tag{D34}$$

The kernel for the quantum spatial search can be given by

$$K(\omega) \equiv \sum_{i} G_{wi}(\omega) = \sum_{i} \sum_{n=0}^{\infty} \gamma^{n} [(\mathbf{G}_{0}(\omega)\mathbf{A})^{n} \mathbf{G}_{0}(\omega)]_{wi}.$$
 (D35)

Here, we have the relation

$$\{[\mathbf{G}_0(\omega)\mathbf{A}]^n\mathbf{G}_0(\omega)\}_{wi} = \{\mathbf{G}_0(\omega)\mathbf{A}[\mathbf{G}_0(\omega)\mathbf{A}]^{n-1}\mathbf{G}_0(\omega)\}_{wi}$$
(D36)

$$=G_{0w}(\omega)\{[\mathbf{AG}_0(\omega)]^n\}_{wi} \tag{D37}$$

For simplicity, we assume that all the degrees for $i \neq w$ is $d_{i(\neq w)} = d$, which provides

$$G_{0i}(\omega) = \frac{1}{\omega + \gamma_w - \gamma d_w} \delta_{iw} + \frac{1}{\omega - \gamma d} (1 - \delta_{iw}) = G_{0w}(\omega) \delta_{iw} + G'(\omega) (1 - \delta_{iw}), \tag{D38}$$

where $G' \equiv G_{0x(\neq w)} = 1/(\omega - \gamma d)$. Using this relation, we have

$$\{[\mathbf{A}\mathbf{G}_{0}(\omega)]^{n}\}_{ij} = \sum_{i_{1}} \cdots \sum_{i_{n-1}} A_{ii_{1}} G_{0i_{1}} A_{i_{1}i_{2}} G_{0i_{1}} \cdots A_{i_{n-2}i_{n-1}} G_{0i_{n-1}} A_{i_{n-1}j} G_{0j}$$

$$= [G'(\omega)]^{n-1} G_{0x}(\omega) \sum_{i_{1}}' \cdots \sum_{i_{n-1}}' A_{ii_{1}} A_{i_{1}i_{2}} \cdots A_{i_{n-2}i_{n-1}} A_{i_{n-1}j}$$

$$+ G_{0w}(\omega) [G'(\omega)]^{n-2} G_{0i}(\omega) \left\{ A_{iw} \sum_{i_{2}}' \cdots \sum_{i_{n-1}}' A_{wi_{2}} \cdots A_{i_{n-2}i_{n-1}} A_{i_{n-1}j} \right\}$$

$$+ \left(\sum_{i_{1}}' A_{ii_{1}} A_{i_{1}w} \right) \sum_{i_{3}}' \cdots \sum_{i_{n-1}}' A_{wi_{3}} \cdots A_{i_{n-1}j} + \cdots \right\}$$

$$+ [G_{0w}(\omega)]^{2} [G'(\omega)]^{n-3} G_{0i}(\omega) \left\{ \cdots \right\} + \cdots ,$$
(D40)

where we used the notation $\sum_{i}' = \sum_{i} (1 - \delta_{iw})$, which represents the sum without i = w.

Let $P_n^k(i,j)$ be the path length distribution with a path length n starting from j to i passing through w k-times. In particular, the path length distribution for the path never through the node w is given by

$$P_n^{(0)}(i,j) = \sum_{i_1}' \cdots \sum_{i_{n-1}}' A_{ii_1} A_{i_1 i_2} \cdots A_{i_{n-2} i_{n-1}} A_{i_{n-1} j}.$$
(D41)

S	quare	lattice
N	400	900
γ	1.66	1.96
P	0.141	0.0760

Hexagonal lattice									
N	400	900							
γ	3.09	3.53							
P	0.0698	0.0423							

Hypercubic lattice											
d	8	9	10	11							
N	2^{8}	2^{9}	2^{10}	2^{11}							
γ	0.161	0.141	0.114	0.104							
P	0.544	0.423	0.800	0.767							

Erdös–Renyi model									
N	400			900					
p	0.1	0.4	1.0	0.1	0.4	1.0			
γ	0.0273	0.00716	0.00310	0.0122	0.00410	$0.00210 \\ 0.0114$			
P	0.871	0.363	0.178	0.461	0.0297	0.0114			

SC(s, s-2)													
s	3				4			5			6		
N	8^{2}	8^{3}	8^{4}	8^{5}	12^{2}	12^{3}	12^{4}	16^{2}	16^{2}	16^{2}	20^{2}	20^{3}	20^{4}
γ	0.470	1.52	2.88	4.57	0.72	2.644	5.92	0.97	4.01	10.5	1.21	5.61	17.25
P	0.597	0.284	0.0764	0.0153	0.48	0.134	0.0201	0.390	0.0720	0.00670	0.324	0.0433	0.00284

	Real complex networks									
	Dolphin[7]	Mouse brain[8]	Co-authorship[9]	Human disease[10]	Facebook[11, 12]					
\overline{N}	62	213	379	516	1446					
γ	1.67	0.0115	2.01	3.05	2.22					
P	0.661	0.990	0.108	0.0617	0.758					

Table IV. Data sets for discussing the relation between the finding probability P and the optimal hopping parameter γ , which is used in Fig. 3 in the main body. SC(s, s-2) represents the Sierpinski carpet with the scaling factor s. The target node is chosen as a node with a minimum degree.

Using this relation, we have

$$\{[\mathbf{A}\mathbf{G}_{0}(\omega)]^{n}\}_{ij} = [G'(\omega)]^{n-1}G_{0y}(\omega)P_{n}^{(0)}(i,j)$$

$$+ G_{0w}(\omega)[G'(\omega)]^{n-2}G_{0j}(\omega)\sum_{m}P_{m}^{(0)}(i,w)P_{n-m}^{(0)}(w,j)$$

$$+ [G_{0w}(\omega)]^{2}[G'(\omega)]^{n-3}G_{0j}(\omega)\sum_{m}\sum_{l}P_{m}^{(0)}(i,w)P_{l}^{(0)}(w,w)P_{n-m-l}^{(0)}(w,j) \cdots$$

$$= \sum_{k}[G_{0w}(\omega)]^{k}[G'(\omega)]^{n-k-1}G_{0j}(\omega)P_{n}^{(k)}(i,j),$$
(D43)

where we used $P_n^{(k+1)}(i,j) = \sum_m P_m^{(0)}(i,w) P_{n-m}^{(k)}(w,j)$. Therefore, we have

$$K(\omega) = \sum_{n=0}^{\infty} \gamma^n \sum_{k} [G_{0w}(\omega)]^k [G'(\omega)]^{n-k-1} \sum_{j} G_{0j}(\omega) P_n^{(k)}(w, j).$$
 (D44)

In short, the finding probability amplitude can be also represented by using the Green's function and the path length distribution.

Appendix E: Relations between the optimal finding probability P and the optimal hopping parameter γ

We here summarize the relations between the optimal hopping parameter γ and the finding probability P. Note that the function $P(t,\gamma)$ was analytically derived for the complete graph [13]. We extend this discussion to the complex networks by employing the WS model, the Sierpinski carpet, the (extended) fractal- β model with the Sierpinski gasket (See Fig. 3 in the main body). In order to produce the data sets for $10^{-2} < \gamma < 10^{0}$, we extend the WS model and fractal- β models by introducing shortcuts [14–16], where edges are added randomly with the probability

 β . The network is regular at $\beta = 0$ and becomes the complete graph at $\beta = 1$ when the number of added shortcuts are sufficient. To analyze the data for the Sierpinski carpet and the (extended) fractal- β model with the Sierpinski gasket, we assumed three fitting functions:

$$f_1(\gamma) \equiv \frac{1}{A + (D\gamma + B)^C},\tag{E1}$$

$$f_2(\gamma) \equiv \frac{1}{A^{\gamma}},$$
 (E2)

$$f_3(\gamma) \equiv \frac{1}{A\gamma^B + C\gamma} \tanh\left(\sqrt{\frac{\gamma}{\gamma + D}}\right),$$
 (E3)

where A, B, C and D are fitting parameters. Here, the parameter D in f_1 is temporarily fixed as D = 1. We evaluated the accuracy of these fitting functions by using the root mean squared percentage error for the fitting function $f_{i=1,2,3}$, given by

$$RMSPE_i = \sqrt{\frac{1}{N} \sum_{j=1}^{N} \left(\frac{P_j - f_i}{P_j}\right)^2},$$
 (E4)

where P_j is the simulation data of the finding probability, the total number of which is N. Results of our simulations are RMSPE₁ = 0.1423, RMSPE₂ = 0.2969 and RMSPE₃ = 0.40178. Therefore, we propose the scaling function f_1 with the fitting parameters A = 0.991(1), B = 0.086(5) and C = 1.68(2). The complete graph gives the relation $P(\gamma = 1/N) \simeq 1$ [5], which is the scope of the scaling function f_1 in the large-N regime.

The scaling function of the (extended) WS model can be given by a variant of f_1 , where the parameter D is now turn to be a fitting parameter, which gives D = 2.11(1). Here, the values of A, B and C are the same as those for the Sierpinski carpet and the (extended) fractal- β model. The scaling function is also useful not only for the theoretical model such as the (extended) fractal- β model including the complete graph, but also real-world complex networks found in the open data [17], such as the co-authorship network [9], human disease network [10] and mouse brain network [8].

We also find network classes where the relation in Eq. (E1) does not work, which are, for example, the Erdös–Renyi random graph, hypercube lattices, fractal Cayley tree [13], T fractal network graph [13], and real complex networks such as dolphin network [7] and Facebook network [11, 12]. The square and hexagonal (honeycomb) lattices are marginal. An interesting expectation is that the difference between two classes may depend on the spectral dimensions. A class of the networks that follows the relation in Eq. (E1) may have the spectral dimension $d_{\rm s} < 2$, whereas other graphs may have the spectral dimensions $d_{\rm s} > 2$, where the behavior of the quantum spatial search is known to change around the critical spectral dimension $d_{\rm s} = 2$ [18–20].

- [1] D. J. Watts and S. H. Strogatz, nature **393**, 440 (1998).
- [2] M. Tomochi, Sociological Theory and Methods 25, 19 (2010).
- [3] K.-I. Goh, B. Kahng, and D. Kim, Phys. Rev. Lett. 87, 278701 (2001).
- [4] A.-L. Barabási and R. Albert, Science 286, 509 (1999).
- [5] A. M. Childs and J. Goldstone, Phys. Rev. A **70**, 022314 (2004).
- [6] M. Newman, Networks: An Introduction (Oxford University Press, Inc., USA, 2010).
- [7] D. Lusseau, Evolutionary ecology **21**, 357 (2007).
- [8] K. Amunts, C. Lepage, L. Borgeat, H. Mohlberg, T. Dickscheid, M.-É. Rousseau, S. Bludau, P.-L. Bazin, L. B. Lewis, A.-M. Oros-Peusquens, N. J. Shah, T. Lippert, K. Zilles, and A. C. Evans, Science 340, 1472 (2013).
- [9] M. E. Newman, Physical Review E 74, 036104 (2006).
- [10] K.-I. Goh, M. E. Cusick, D. Valle, B. Childs, M. Vidal, and A.-L. Barabási, Proceedings of the National Academy of Sciences 104, 8685 (2007).
- [11] A. L. Traud, E. D. Kelsic, P. J. Mucha, and M. A. Porter, SIAM Rev. 53, 526 (2011).
- [12] A. L. Traud, P. J. Mucha, and M. A. Porter, Phys. A 391, 4165 (2012).
- [13] E. Agliari, A. Blumen, and O. Muelken, Physical Review A 82, 012305 (2010).
- [14] R. Monasson, The European Physical Journal B Condensed Matter and Complex Systems 12, 555 (1999).
- [15] M. Newman and D. Watts, Physics Letters A 263, 341 (1999).
- [16] M. E. Newman, SIAM review **45**, 167 (2003).
- [17] R. Rossi and N. Ahmed, Proceedings of the AAAI Conference on Artificial Intelligence 29 (2015).
- [18] S. Tamegai, S. Watabe, and T. Nikuni, Journal of the Physical Society of Japan 87, 085003 (2018).

- [19] A. Patel and K. S. Raghunathan, Phys. Rev. A $\bf 86$, 012332 (2012). [20] R. Sato, T. Nikuni, and S. Watabe, Physical Review A $\bf 101$, 022312 (2020).